

Modeling of Impurity Transport in the Divertor of JET^{*})

Andreas KIRSCHNER¹⁾, Dmitry MATVEEV^{1,2)}, Mathias GROTH³⁾, Sebastijan BREZINSEK¹⁾, Vladislav KOTOV¹⁾, Karl KRIEGER⁴⁾, Dmitry BORODIN¹⁾, Carolina BJÖRKAS^{1,5)}, Markus AIRILA⁶⁾, Hans G. ESSER¹⁾, Gennady SERGIENKO¹⁾, Ulrich SAMM¹⁾ and JET EFDA CONTRIBUTORS^{7,†)}

¹⁾*Institut für Energie- und Klimaforschung – Plasmaphysik, Forschungszentrum Jülich, Association EURATOM-FZJ, Trilateral Euregio Cluster, 52425 Jülich, Germany*

²⁾*Department of Applied Physics, Gent University, Rozier 44, B-9000 Gent, Belgium*

³⁾*Aalto University, Association EURATOM-Tekes, Espoo, Finland*

⁴⁾*Max-Planck-Institut für Plasmaphysik, EURATOM Association, 85748 Garching, Germany*

⁵⁾*EURATOM-Tekes, Department of Physics, P.O.B 64, 00014 University of Helsinki, Finland*

⁶⁾*VTT Technical Research Centre of Finland, Association EURATOM-Tekes, 02044 VTT, Finland*

⁷⁾*JET-EFDA, Culham Science Centre, Abingdon, OX14 3DB, UK*

(Received 6 December 2012 / Accepted 4 March 2013)

Deposition/erosion measurements by means of a Quartz Micro Balance (QMB) located below the Load Bearing Septum Replacement Plate in the private flux region of the inner divertor of JET (with full carbon wall) revealed net deposition with the inner strike point located on the vertical tile and net erosion with the inner strike point on the horizontal tile [H.G. Esser *et al.*, J. Nucl. Mater. **390–391**, 148 (2009)]. ERO calculations show about 3.5 times larger flux entering the QMB aperture when the inner strike point is located on the vertical plate compared to the case when strike point is on the horizontal plate – thus indicating similar behavior. Using these fluxes from ERO as input, detailed modeling of erosion/deposition at the QMB itself considering the realistic geometry of the QMB housing has been performed with the 3D-GAPS code. The QMB measurements can be reproduced with combined ERO/3D-GAPS modeling if erosion due to deuterium atoms within the QMB housing is taken into account.

© 2013 The Japan Society of Plasma Science and Nuclear Fusion Research

Keywords: JET, divertor, erosion, deposition, impurity transport, Quartz Micro Balance, plasma-wall interaction

DOI: 10.1585/pfr.8.2402038

1. Introduction

Erosion of wall components, subsequent transport of eroded impurities and resulting deposition are critical issues for the development of a fusion reactor. The life time of wall components will be limited by erosion processes. In addition, co-deposition of radioactive tritium in deposited layers has to be reduced as much as possible since the in-vessel amount of tritium has to stay below a certain value for safety reasons (e.g. 1 kg in the case of ITER). After reaching this limit, time consuming and expensive measures have to be undertaken to clean the device. Thus, both wall life time and long-term tritium retention will determine the availability of future fusion devices. Long-term tritium retention is in particular expected in remote, plasma-shadowed areas of the fusion device [1]. It is therefore important to understand layer formation in remote areas to make predictions for future devices.

Within the present work erosion and deposition is

studied in the private flux region (PFR), thus remote area of the inner divertor of JET under carbon wall conditions. Measurements with a Quartz Micro Balance (QMB) diagnostic located below the Load Bearing Septum Replacement Plate (LBSRP) in the inner PFR are compared with detailed modeling of erosion, impurity transport and re-deposition.

2. Erosion and Deposition in the Inner Private Flux Region of JET

2.1 Quartz Micro Balance measurements

Erosion and deposition measured on the QMB crystal located below the LBSRP has been published in [2]. The QMB diagnostic makes use of the resonance frequency change of a quartz crystal with its mass. As the frequency also depends on temperature, a second quartz is installed in the QMB housing, protected from plasma impact to discriminate frequency changes due to mass and due to thermal effects. The principle of the QMB diagnostics at JET and the sensitivity of the system are explained in [3]. The QMB below the LBSRP was mounted behind a gap-like

author's e-mail: a.kirschner@fz-juelich.de

^{*}) This article is based on the invited presentation at the 22nd International Toki Conference (ITC22).

[†]) See the Appendix of F. Romanelli *et al.*, Proceedings of the 24th IAEA Fusion Energy Conference 2012, San Diego, USA

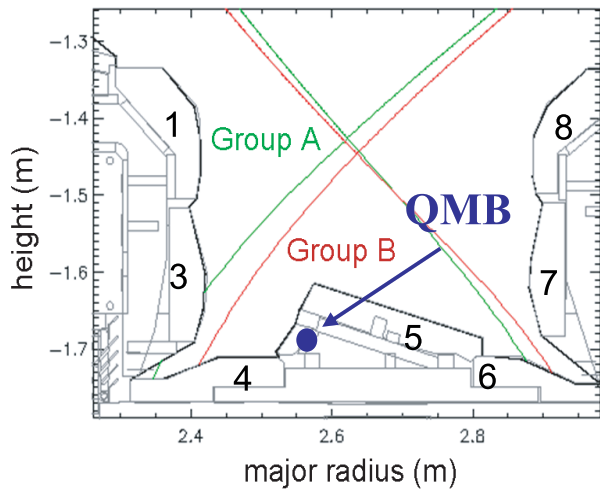


Fig. 1 Geometry of the inner divertor of JET. The location of the QMB below the LBSRP (tile 5) is indicated and the positions of the strike points for discharges of group A and group B are shown.

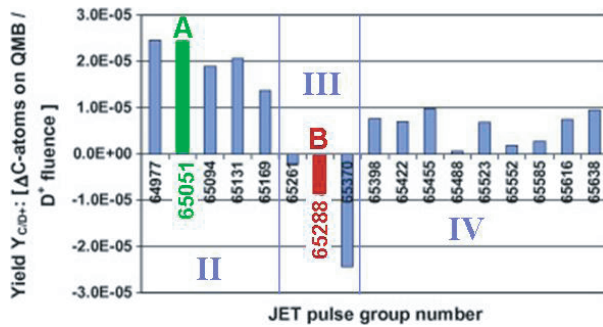


Fig. 2 Measured deposition and erosion on the QMB in dependence on the discharge group.

aperture (recessed by 4.5 cm from the front surface of the protection tile) with the aperture providing a line-of-sight view to the vertical tiles 1 and 3, but only partly to the horizontal tile 4 – compare Fig. 1. The measurements have been performed during the restart phase of JET in 2006 with full carbon wall and applying successive discharges with moderate additional heating (2-3 MW) and various plasma configurations. Due to the high discharge repetition rate, the QMB crystal did not reach thermal equilibrium on a shot-to-shot base. Therefore, data were only measured in the morning before plasma operation providing erosion/deposition information mostly on a daily basis and thus averaged over a group of discharges. Figure 2 shows measured deposition/erosion as yield Y_{C/D^+} of carbon atoms deposited/eroded on the QMB crystal per incident deuterium ion impacting onto a toroidal section of 1 cm length of the inner divertor (the same toroidal extension as the QMB). The deuterium ion flux was measured by D_α light emission. Analysis of the discharges within each group revealed that deposition on the QMB is observed when the inner strike point mainly was located on

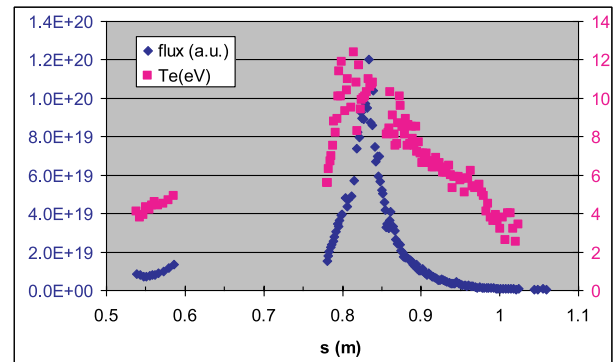


Fig. 3 Langmuir probe measurements of plasma temperature and saturation current along tile 3 for JET L-mode discharge #68126. The maximum of flux corresponds to the location of the strike point.

the vertical tile 3, whereas erosion was observed when the strike point was on tile 4, see Table 1 in reference [2]. The scattering in the measurements can be explained by varying plasma conditions (e.g. heating power) and the fact that the strike point normally was not exclusively located at the same tile for all discharges within a group.

2.2 Modeling with ERO and 3D-GAPS

The three-dimensional impurity transport and plasma-wall interaction code ERO [4] is applied to model the transport of eroded particles within the inner divertor region. To address the detailed transport of impurities within the QMB housing, taking into account the real geometry, the 3D-GAPS code [5] is used. The flux of carbon and hydrocarbon particles entering the QMB aperture modeled with ERO is used as input for 3D-GAPS.

Two groups of discharges have been chosen for the modeling as indicated in Fig. 2 – group A representing the situation of the inner strike point located (mainly) on the vertical plate 3 and group B with the inner strike point (mainly) on horizontal tile 4. The discharges within these groups were performed under rather similar plasma conditions (except of strike point location) and in general were quite reproducible. Detailed analysis of the D^+ fluence distributions of these discharge groups show the following partition, see Figs. 5 (a) and (b) in reference [2]:

- D^+ fluence for group A: about 91% on tile 3 and about 9% on tile 4
- D^+ fluence for group B: about 12% on tile 3, about 86% on tile 4 and about 2% on tile 1

The inner strike point positions within the ERO modeling are fixed to one position according to the D^+ fluence distribution on the vertical tile 3 for group A and on the horizontal tile 4 for group B. No measurements of plasma parameters are available during the restart phase and thus also no plasma simulations. Therefore a simplified approach is undertaken within this work by defining the plasma electron temperature and density at the

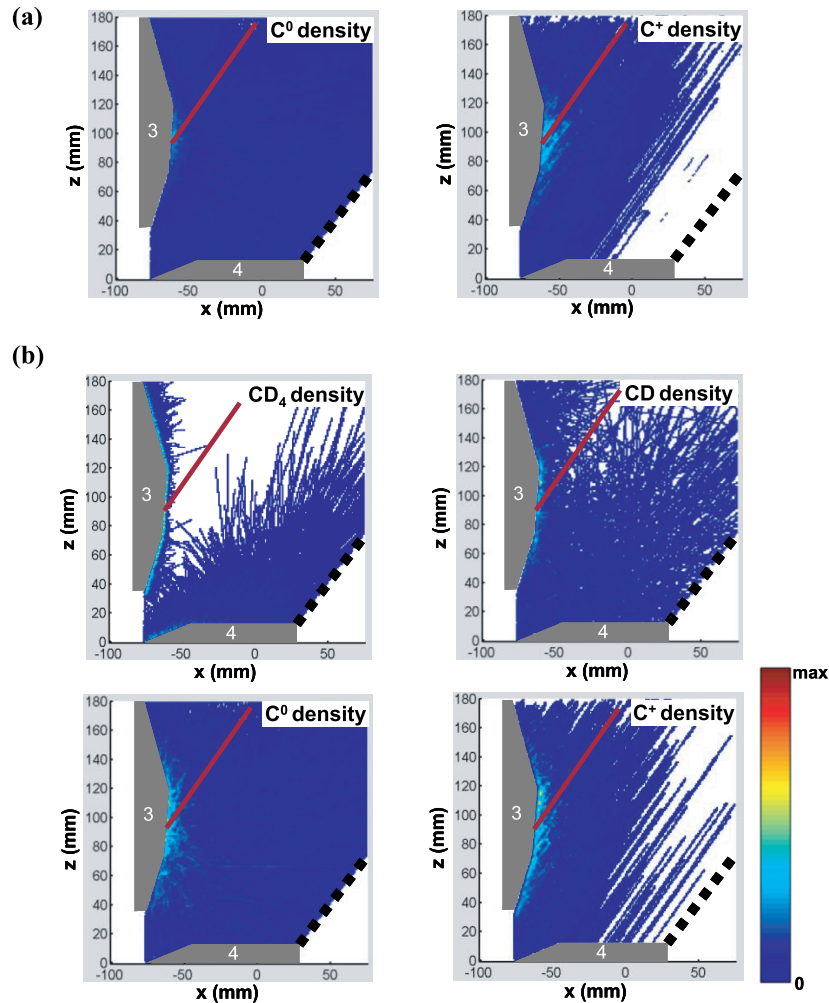


Fig. 4 Strike point on vertical tile 3: (a) C⁰ and C⁺ distribution from physical sputtering. (b) CD₄, CD, C⁰ and C⁺ distribution from chemical erosion. The red lines indicate the separatrix. The color map for each figure is scaled to the respective maximum intensity of density.

position of the inner strike point assuming typical values for low power discharges at JET ($T_e = 10$ eV and $n_e = 1 \cdot 10^{13}$ cm⁻³). Perpendicular to the separatrix an exponential decay of the plasma parameter is assumed. The decay lengths within the scrape-off-layer (SOL) and the PFR are taken from Langmuir probe measurements of the electron temperature and ion flux during an L-mode discharge #68126 shown in Fig. 3. An evaluation of these data reveals the following decay lengths: $\lambda_T(\text{SOL}) = 160$ mm, $\lambda_T(\text{PFR}) = 60$ mm, $\lambda_n(\text{SOL}) = 40$ mm, $\lambda_n(\text{PFR}) = 40$ mm. The decay lengths for the density have been calculated under the assumption of $\Gamma \sim n \cdot T^{0.5}$. The plasma parameters are assumed to be constant along the toroidal direction. Also, the flow velocity is assumed to be constant (acoustic sound speed) along the magnetic field lines. Cross-field diffusion is considered with a constant coefficient of 0.2 m²/s.

2.2.1 ERO modeling results

Strike point located on the vertical tile 3 (corresponding to discharge group A):

For clarity physical sputtering and chemical erosion are treated separately. Figure 4 (a) presents the distribution of carbon atoms C⁰ and ions C⁺ resulting from physical sputtering. The ERO simulation volume is restricted to the inner divertor; the y-axis corresponds to the toroidal direction of JET. The strike point is located at $z = 90$ mm on the vertical tile 3. Particles leaving the simulation volume in z_{max} -direction are lost for the simulation as their probability to re-enter the simulation volume is assumed to be small. The same is true for particles leaving the simulation volume in x_{max} -direction with z -coordinates above the dashed line indicated in the figure. This dashed line corresponds to the area below the LBSRP tile – particles crossing this line are stored and used as input for the 3D-GAPS modeling. The ionized species gyrate along the magnetic field lines (which are directed mainly in toroidal direction, i.e. perpendicular to the x, z plane shown in Fig. 4) and

thus move within the magnetic flux surfaces as seen in the figure. The erosion and re-deposition profiles from physical sputtered particles along the inner divertor tiles are shown in Fig. 5 (a). The cell numbering along the surface starts at the top of vertical tile 3 ($z = 180$ mm) and ends

at the horizontal tile 4 ($x = 29$ mm). About 54% of physically sputtered carbon is re-deposited on the divertor tiles. Figure 4 (b) presents the distribution of chemically eroded CD_4 and also CD , C^0 and C^+ resulting from dissociation and ionization. For chemical erosion of carbon a yield $Y_{chem} = 1\%$ has been assumed considering the formation of methane CD_4 . Resulting erosion and re-deposition profiles are shown in Fig. 5 (b). The fraction of re-eroded material which is re-deposited on the tiles is 63% for chemical erosion, which is slightly larger than for physical sputtering.

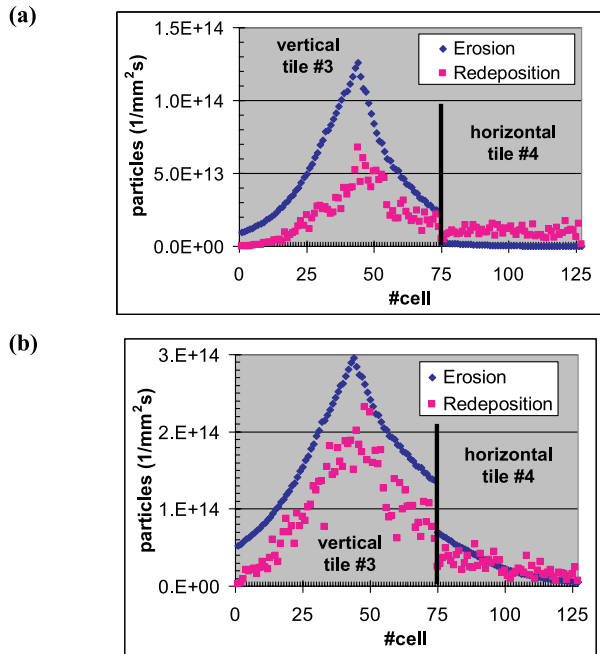


Fig. 5 Strike point on vertical tile 3: (a) Erosion and re-deposition profile from physical sputtering. (b) Erosion and re-deposition profile from chemical erosion.

Strike point located on the horizontal tile 4 (corresponding to discharge group B):

Figure 6 shows eroded species from physical sputtering and chemical erosion with the strike point located at $x = -63$ mm on the (sliding part of) horizontal tile 4. Resulting erosion and re-deposition profiles are presented in Fig. 7. The fraction of re-deposition along the tiles is 47% for physical sputtering and 61% for chemical erosion and thus slightly smaller compared to the simulation with the strike point on the vertical plate 3.

Estimated carbon flux to QMB aperture:

From the above-described modeling the flux of carbon species entering the QMB aperture has been estimated and summarized in Table 1. The results are also given as ratio $Y_{C/D+}(ERO)$ to the deuterium fluence to compare with the measured deposition/erosion yield $Y_{C/D+}(EXP)$ on the QMB (the last column of the table). It is seen that the dominating part of the flux entering the QMB aperture origi-

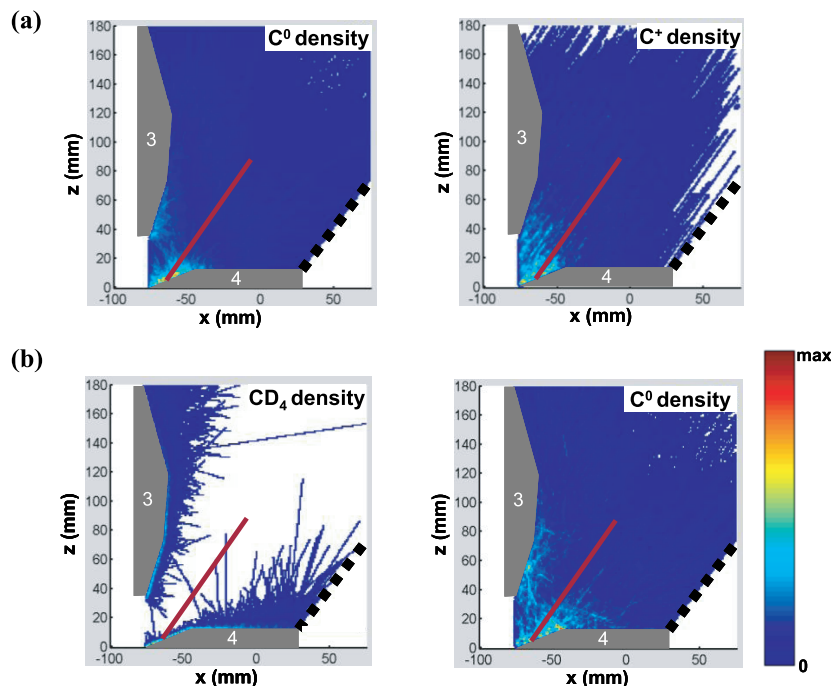


Fig. 6 Strike point on horizontal tile 4: (a) C^0 and C^+ distribution from physical sputtering. (b) CD_4 and C^0 distribution from chemical erosion. The red lines indicate the separatrix. The color map for each figure is scaled to the respective maximum intensity of density.

Table 1 Modeled amount of carbon particles entering the QMB aperture, $Y_{C/D+}$ (ERO), in comparison to measured deposition/erosion on the QMB, $Y_{C/D+}$ (EXP). Two groups of discharges with different locations of the inner strike point (SP) are considered.

| | | C particles per s to QMB aperture (ERO) | C particles to QMB aperture $Y_{C/D+}$ (ERO) | Deposition/Erosion on QMB $Y_{C/D+}$ (EXP) |
|------------------------|---------------------|---|--|--|
| SP on tile 3 (group A) | Physical sputtering | $2.8 \cdot 10^{16}$ | $+3.0 \cdot 10^{-3}$ | $+2.4 \cdot 10^{-5}$ |
| | Chemical erosion | $6.0 \cdot 10^{16}$ | | |
| SP on tile 4 (group B) | Physical sputtering | $3.0 \cdot 10^{15}$ | $+8.9 \cdot 10^{-4}$ | $-0.9 \cdot 10^{-5}$ |
| | Chemical erosion | $2.0 \cdot 10^{16}$ | | |

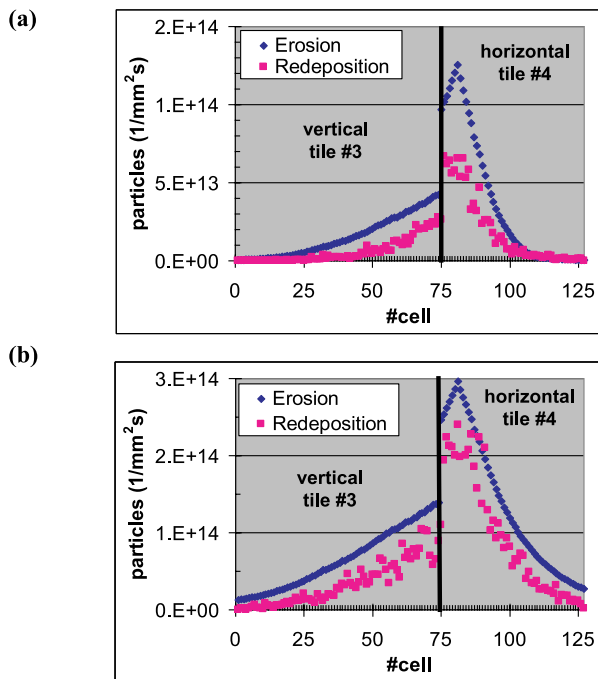


Fig. 7 Strike point on horizontal tile 4: (a) Erosion and re-deposition profile from physical sputtering. (b) Erosion and re-deposition profile from chemical erosion.

rates from chemical erosion, which is in particular true for the case with the strike point on the horizontal tile 4. Also, the modeling gives about 3.5 times larger flux to the QMB aperture with the strike point on tile 3 (group A) compared to the case with the strike point on tile 4 (group B). As the QMB shows deposition in group A and erosion in group B the ERO results tend in the right direction. However, the resulting deposition/erosion on the QMB will be addressed in the next section with 3D-GAPS modeling.

Further ERO simulations have been performed assuming an enhanced (compared to bulk carbon) re-erosion of re-deposited carbon at the divertor tiles. Such enhancement at plasma-wetted areas has been discussed in the literature; see e.g. Ref. [6–8]. To study the effect on the modeling ten times enhanced physical sputtering and chemi-

cal erosion is assumed. It is seen that the erosion flux increases by about a factor of 2 compared to the simulations without enhancement. This increase is smaller than the enhancement factor as the concentration of re-deposited carbon (which suffers from enhanced re-erosion) in the surface under steady state conditions is smaller than 100%. The modeled flux to the QMB aperture increases correspondingly by a factor of 2 compared to the case without enhanced re-erosion.

2.2.2 3D-GAPS modeling

The detailed geometry of the QMB housing is considered by 3D-GAPS. The amount, species and 3D velocity distribution of particles entering the QMB aperture of the housing is taken from the above-described ERO modeling. ERO shows that only neutral carbon and hydrocarbon species are able to enter the QMB aperture whereas ions, travelling mainly along the magnetic field lines, are not able to enter. Within the QMB housing the carbon impurity transport is calculated considering reflection at the inside surfaces of the housing and erosion due to neutral deuterium entering the QMB aperture. Physical sputtering due to carbon species entering the QMB housing is also considered. The flux of deuterium atoms entering the QMB aperture is an input parameter for 3D-GAPS and is varied between $1 \cdot 10^{17}$ and $1 \cdot 10^{19} \text{ cm}^{-2} \text{ s}^{-1}$ in the present work. Transport of deuterium atoms within the QMB housing is treated in a similar way as to carbon. Figure 8 summarizes the resulting modeled deposition/erosion on the QMB crystal with respect to its dependence on the deuterium atom flux entering the QMB aperture. With a chemical erosion yield for deuterium atoms of 1% (open circles), a deuterium atom flux density at the QMB aperture of about $1 \cdot 10^{18} \text{ cm}^{-2} \text{ s}^{-1}$ is necessary to reproduce the measured deposition for group A (SP on vertical tile 3) and erosion for group B (SP on horizontal tile 4). Assuming a larger chemical erosion yield of 5% (stars in Fig. 8) reduces the necessary atom flux to about $2 \cdot 10^{17} \text{ cm}^{-2} \text{ s}^{-1}$. The results shown in Fig. 8 correspond to ERO simulations without the assumption of enhanced re-erosion of re-deposits. As the carbon flux entering the QMB aperture increases with en-

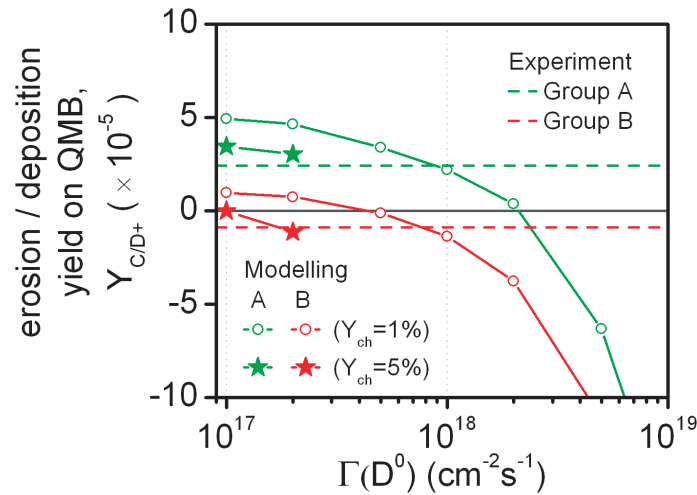


Fig. 8 Modeled deposition/erosion on the QMB crystal for discharge groups A and B as a function of the deuterium atom flux entering the QMB aperture: open circles for an assumed chemical erosion of 1% and stars for a chemical erosion of 5%. The dashed lines indicate the measurements.

hanced re-erosion, larger deuterium atom fluxes have to be assumed to match the experimentally observed deposition/erosion on the QMB.

No certain information about atomic fluxes is available for the discharges in questions. However, B2-EIRENE simulations made for configuration of #50401 with septum (JET MkIIIGB) and strike points on the vertical targets [9] show that for a scrape-off layer input power of 2.5 MW the D atom flux at the QMB location varies between $\sim 1 \cdot 10^{17}$ and $\sim 6 \cdot 10^{17} \text{ cm}^{-2} \text{ s}^{-1}$ depending on the discharge density. In Ref. [10] it is seen that the divertor neutral pressure for discharges at low densities (as have been applied for the discharges of the restart phase discussed within the present paper) is similar for JET MkIIIGB and MkIIA, whereas the latter configuration is more similar to the one with LBSRP. It also has to be noted that the neutral pressure in the divertor is typically larger when the strike point is located on the horizontal plate compared to the strike point located on the vertical plate (factor 2-4). However, in conclusion, the values derived for the neutral flux to the QMB aperture are in the same order of magnitude as the ones which have to be assumed for the 3D-GAPS modeling.

3. Conclusion and Outlook

Combined ERO/3D-GAPS modeling can reproduce the general tendency of erosion and deposition measured with the QMB located below the LBSRP in the inner divertor of JET. However, due to limited data acquisition during the restart phase, in which the presented QMB data have been measured, no detailed information is available about the plasma parameters and deuterium atom fluxes. Therefore, generic, yet representative plasma parameters and

certain deuterium atom flux entering the QMB aperture have been assumed for the modeling to compare with the deposition/erosion measured on the QMB. This approach led to reasonable results and motivates further modeling and experiments. Thus, in the future additional modeling is planned to study deposition/erosion on the QMB crystals located in the inner and outer divertor of JET within dedicated discharges during the upcoming campaign under ITER-like wall conditions. Also spectroscopic measurements of impurity transport can then serve as additional information for benchmarking the modeling results.

Acknowledgments

This work, supported by the European Communities under the contract of Association between EURATOM/FZJ, was carried out within the framework of EFDA. The views and opinions expressed herein do not necessarily reflect those of the European Commission. CPU time for computations has been provided by JSC (Jülich Supercomputer Centre).

- [1] T. Loarer, *J. Nucl. Mater.* **390–391**, 20 (2009).
- [2] H.G. Esser *et al.*, *J. Nucl. Mater.* **390–391**, 148 (2009).
- [3] H.G. Esser *et al.*, *Fusion Eng. Des.* **66–68**, 855 (2003).
- [4] A. Kirschner *et al.*, *Nucl. Fusion* **40**, 989 (2000).
- [5] D. Matveev *et al.*, *Plasma Phys. Control. Fusion* **52**, 075007 (2010).
- [6] A. Kirschner *et al.*, *J. Nucl. Mater.* **328**, 62 (2004).
- [7] A. Kirschner *et al.*, *J. Nucl. Mater.* **415**, S239 (2011).
- [8] R.P. Doerner *et al.*, *Nucl. Fusion* **52**, 103003 (2012).
- [9] V. Kotov *et al.*, *J. Nucl. Mater.* in press, DOI: 10.1016/j.jnucmat.2013.01.091.
- [10] A. Loarte, *Plasma Phys. Control. Fusion* **43**, R183 (2001).